Progress In Electromagnetics Research M, Vol. 110, 133–143, 2022

A New 2 × 2-Element Subarray Antenna Synthesis Based on Waveguide Cavity Resonators

Raad S. Jarjees[1] and Rashad H. Mahmud[2, 3, *]

Abstract—A new design of a 2×2-element subarray antenna based on an all-cavity resonator structure is presented in this article. A novel topology which employs only two resonators to lay out the subarray is proposed, and two X-band rectangular waveguide cavity resonators are utilized for the subarray physical implementation. The first resonator is a conventional half-guided resonator operating at the TE_{101} mode. The second resonator, which is an oversized TE_{102} resonator based, is modified in order to keep the TE_{101} mode to propagate within the bandwidth of interest and facilitate the connection with four radiating apertures. The developed coupling matrix approach is utilized to calculate the desirable frequency response, which is a standard 2^{nd} order Chebyshev response with introducing filtering functionality to the realised gain response of the subarray. The simulation results obtained by two simulation softwares (CST and Ansoft HFSS) validate the calculation results. An extremely wide impedance bandwidth of 23% at center frequency 10 GHz when the reflection coefficient $S_{11} = -10$ dB is obtained. A very stable realised gain with less than 0.5 dBi variations over the bandwidth of interest (8.8–11.1 GHz) is obtained with a peak gain value of 13.1 dBi at 11 GHz. The radiation patterns have very low side lobe levels, particularly in the E-plane, due to the existence of small non-radiating area and maintaining small spacing between the radiating apertures. The proposed 2×2-element subarray has the advantages of wider bandwidth and low profile compared with our and other previous 2×2-element subarrays.

1. INTRODUCTION

A high speed data rate capability of a modern wireless communication link is demanded when it operates at long-distance applications in order to allow a rapid transmission of data simultaneously [1]. To fulfill this demand, a high gain and wide bandwidth antenna needs to be employed at the system. Due to their inherent low transmission losses and high energy handling, hollow slotted waveguide antenna arrays have been widely employed in many microwave and millimeter-wave wireless communication systems [2].

A conventional slotted waveguide antenna array, which is usually built from a single waveguide-layer, has employed a series-feed network technique to feed the array elements. Although such a feed-network has numerous advantages of low profile and mass productivity, it limits the array bandwidth due to long-line effect [3]. A partially-corporate feed approach presented in [4] has the potential of minimising the long-line effect and then enhancing the waveguide array bandwidth. However, this approach introduces non-radiating area to the radiation side of the arrays and degrades the side lobe levels of the radiation patterns. A full-corporate feed approach presented in [3] was extremely effective to enhance the bandwidth, particularly for the larger waveguide arrays. It is based on splitting the whole array into a number of 2×2-element subarrays and feeding them from beneath using a series of T- and H-plane junctions [1, 5–12]. This approach costs an extra waveguide-layer and increasing the

Received 1 March 2022, Accepted 29 April 2022, Scheduled 12 May 2022

* Corresponding author: Rashad Hassan Mahmud (rhm112@alumni.bham.ac.uk).

[1] Physics Department, University of Zakho, Iraq. [2] Physics Department, Salahaddin University-Erbil, 44002, Iraq. [3] Mechatronics Engineering, Faculty of Engineering, Tishk International University, Erbil 44001, Iraq.

array volume. To keep low profile of the array and enhance the bandwidth, overload and open cavities techniques were presented in [13]. Although these techniques do not cost extra layers, the amount of the enhancement may not be sufficient to meet the demands of many modern wireless systems.

More recently, we have developed the coupling matrix approach for the design of antenna arrays using rectangular waveguide cavity resonators [14–17]. The approach has allowed the arrays to be built out of sole resonators. The advantages of this approach over the other presented approaches are to give controllable bandwidth to the arrays and remove the need of a separate feed network design without costing extra layer [14]. Also, the antenna gain is extremely stable over the band of interest regardless of its operating frequency band. To achieve all these, appropriate topologies have to be chosen for the arrays. It should be mentioned that the criteria used to choose the topologies for the antenna arrays are based on occupying less area, utilizing fewer resonators, and keeping larger roll-off of the realised gain at the band edges as much as the wireless link is demanded. In [16], we have presented two topologies, which consist of 6 and 7 resonators, for the design of 2×2-element subarrays using the coupling matrix approach.

In this paper, we develop the design of a 2×2-element subarray based on all resonator structure one step further to miniaturize the size, enlarge the bandwidth, and keep the high radiation performance. To do this, a novel topology has been proposed which is based on only two resonators. Such topology offers significant reduction of the subarray size. Two different physical configurations of rectangular waveguide cavity resonators are utilized to interpret the topology into the physical structure. The coupling matrix approach is coded in the numerical analysis (MATLAB) software in order to extract the coupling coefficient and quality factors of the resonators, and also to obtain the calculated results. The proposed 2×2-element subarray is designed using the Computer Simulation Technology (CST) and Anosft High-Frequency Structure Simulator (HFSS) studios. The simulated results are compared with the calculations in order to verify the approach.

2. ANTENNA DESIGN

2.1. Coupling Matrix Theory

Originally, the coupling matrix theory was presented as a technique for the design of two-port narrow-bandwidth Bandpass Filters (BPFs) based on waveguide cavity resonators [18, 19]. It represents the BPFs in terms of an $n \times n$ general matrix $[A]$, where n is the number of coupled-resonators. One of the advantages of this approach is that each element of the matrix represents a specific physical section of the coupled-resonators employed in the BPF. This helps to achieve the desired frequency specifications for the BPFs. Later, this approach was developed for the multiple-port circuit designs such as multiplexers and power splitters [20, 21]. More recently, we have developed the approach for the antenna array designs [14–16]. Here, similar to the BPFs design, an antenna array is considered to be designed based on sole coupled-resonators in order to represent it in terms of the general matrix $[A]$ as expressed as follows:

$$[A] = \begin{bmatrix} \frac{1}{q_{e1}} & \cdots & 0 & 0 \\ \vdots & \ddots & \vdots & \vdots \\ 0 & \cdots & \ddots & \vdots \\ 0 & \cdots & \vdots & \frac{1}{q_{rn}} \end{bmatrix} + p \begin{bmatrix} 1 & \cdots & 0 & 0 \\ \vdots & \ddots & \vdots & \vdots \\ 0 & \cdots & 1 & \vdots \\ 0 & \cdots & \vdots & 1 \end{bmatrix} - j \begin{bmatrix} m_{11} & \cdots & m_{1(n-1)} & m_{1n} \\ \vdots & \ddots & \vdots & \vdots \\ m_{(n-1)1} & \cdots & m_{(n-1)(n-1)} & m_{(n-1)n} \\ m_{n1} & \cdots & \vdots & m_{nn} \end{bmatrix} \quad (1)$$

Or

$$[A] = [q] + p\,[U] - j\,[m]$$

where (q_{e1}) is the scaled external quality factor of resonator 1 which is coupled to the input port. q_{rn} is the scaled radiation quality factor of resonator n which lunches the Electromagnetic (EM) radiation into space. The q_{e1} and q_{rn} values can be calculated using the relations: $q_{e1} = g_0 g_1$, $q_{rn} = g_n g_{n+1}$ [22]. g_0, g_1, and g_n are the element values of the Chebyshev low pass prototype filters which can be calculated using the relations given in [22]. p is a complex frequency variable which is related to the antenna fractional bandwidth (FBW), band edges angular frequency (ω), and angular center frequency (ω_0) by

$p = j/\text{FBW}(\omega/\omega_0 - \omega_0/\omega)$, respectively. m_{ij} is the scaled coupling coefficient between the coupled resonators i and j. The scaled reflection coefficient (S_{11}) of the antenna array may be expressed by:

$$S_{11} = \pm\left(1 - \frac{2}{q_{e1}}[A]^{-1}_{11}\right) \tag{2}$$

where the signs ($\pm$) refer to the coupling types between the coupled resonators [22]. S_{11} magnitude is usually expressed in unit of decibel (dB) in the calculation. It is crucial to mention here that the antenna q_{e1} and q_{rn} quality factors have to be equal to each other, i.e., $q_{e1} = q_{r1} = q_{r2} \cdots = q_{rn}$ so as to maintain the desirable impedance matching over the bandwidth of interest. The coupling matrix approach is usually utilized in order to introduce the high frequency selectivity at start and stop bands of the antenna gain performance [15, 16, 20]. The main focus here is to utilize it in order to enlarge the antenna bandwidth and minimise the antenna size.

It is worth mentioning that n-coupled resonators could be employed in the BPF or filtering antenna circuits. However, employed more resonators leads to increasing the circuits' size and reducing the interest of the design. Therefore, for the proposed 2×2-element subarray shown in Fig. 1, only two resonators are employed. The general $[A]$ matrix given in Equation (1) can be simplified after choosing the topology specifications ($f_0 = 10\,\text{GHz}$, FBW $= 0.23$ (or 23%) when $S_{11} = -10\,\text{dB}$) and using the gradient-based optimization technique [14, 20], as follows:

$$[A] = \begin{bmatrix} 0.7610 & 0 \\ 0 & 0.7610 \end{bmatrix} + p\begin{bmatrix} 1 & 0 \\ 0 & 1 \end{bmatrix} - j\begin{bmatrix} 0 & 0.2597 \\ 0.2597 & 0 \end{bmatrix} \tag{3}$$

It is important to mention that the self-couplings (m_{11}, m_{22}), source-load couplings (m_{SL}, m_{LS}), and cross-couplings between the radiating ports are neglected in the computation of the $[A]$ matrix in order to simplify the calculations. After finding the $[A]$ matrix (Equation (3)) and inserting it into Equation (2), the calculated S_{11} response can be computed. Also, the matrix elements (m_{12}, $q_{e1} = q_{rn}$) values in Equation (3) can be used to interpret the physical dimensions of the configuration shown in Fig. 1(b). These are handled in Sections 2.2 and 2.3.

2.2. Antenna Topology and Physical Configuration

The novel topology proposed for the 2×2-element subarray antenna is presented in Fig. 1(a). It consists of only two resonators. Resonator 1, which is coupled to the input port and denoted by the black node, acts as a feed network and introduces the frequency filtering functionality to the subarray. Resonator 2,

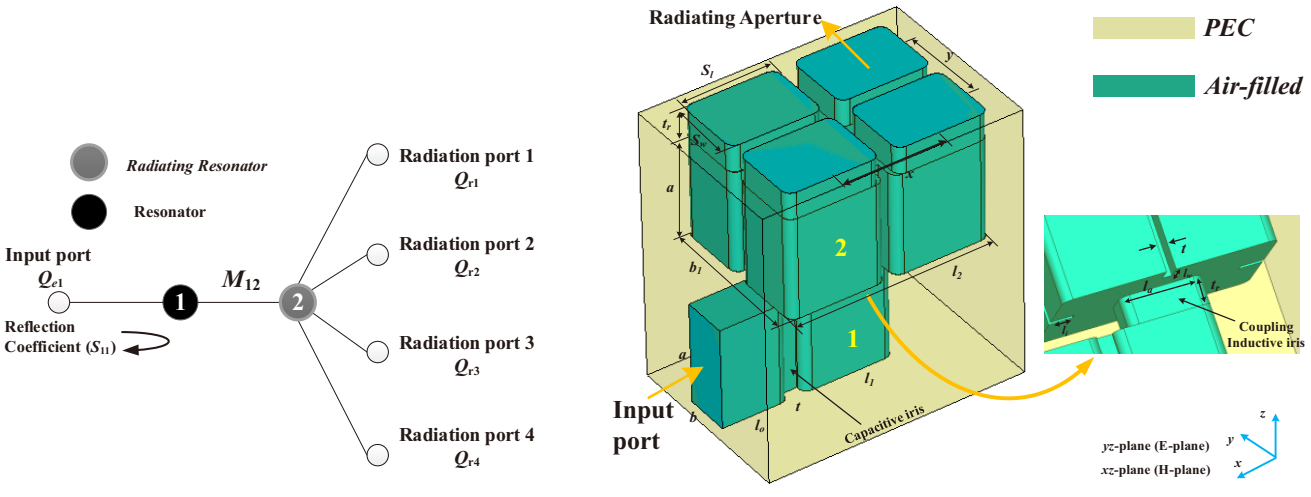

(a) (b)

Figure 1. (a) The topology, and (b) physical configuration of the 2×2-element subarray topology using perfect electrical conductor (PEC) in CST.

which is called radiating resonator (grey node), serves as a radiator in addition to its frequency filtering functionality role. It couples to space through four radiating ports. The proposed subarray is designed to operate at X-band frequencies with the center frequency of $f_0 = 10\,\text{GHz}$ and having FBW $= 0.23$ (or 23%) when $S_{11} = -10\,\text{dB}$.

The physical configuration of the 2×2-element subarray shown in Fig. 1(b) is based on only two rectangular waveguide cavity resonator structures. Resonator 1, which is a conventional TE_{101} rectangular cavity resonator, has a length about half-guided wavelength ($l_1 \approx 0.5\lambda_g$). It couples to the input port via the capacitive iris from one side, while it couples to the radiating resonator from beneath via an inductive iris in order to ease the physical configuration. Originally, the radiating resonator is TE_{102} rectangular cavity resonator based. It has a length of about one-guide wavelength ($l_2 \approx 1\lambda_g$) and a width (b_1) which is double of the conventional waveguide ($b_1 \approx 2b$). It should be mentioned that the TE_{102} rectangular cavity resonator employed in the design with the given dimensions facilitates the connections of the radiating resonator with the four radiating outputs. The resonant frequencies (f_{nml}) of the cavities can be calculated using the cavity mode equation [23]:

$$f_{nml} = \frac{c}{2\pi}\sqrt{\left(\frac{m\pi}{a}\right)^2 + \left(\frac{n\pi}{b}\right)^2 + \left(\frac{l\pi}{d}\right)^2} \tag{4}$$

Here, c is the speed of light in vacuum, and a, b, and d are physical dimensions of the cavities. n, m, and l are integer numbers used to represent the electric and magnetic field modes inside the cavities.

Unlike the TE_{101} mode cavity resonator (Fig. 2(a)), the TE_{102} mode cavity usually creates two out-of-phase electric field loops (complete wave) inside the waveguide [23, 24], as illustrated in Fig. 2(b). Also, the surface electric field current lines created by the electric filed loops on the waveguide side walls are out-of-phase as well. The current lines will not excite the four radiating apertures all in phase, and then a destructive radiation pattern would be produced. To remedy this, four capacitive irises are etched into the broad-walls of the radiating resonators. The irises dimensions (l_i, l_w) are manipulated to keep only the TE_{101} mode to propagate within the operating frequency band 8–12 GHz. As obtained from the CST simulator and shown in Fig. 3, the E-field current lines are distributed homogenously and all in-phase around the corners of the radiating resonator within the operating frequency bandwidth of interest (9–11 GHz). This makes the corners of the resonator to be the perfect positions to locate the four radiating apertures on it.

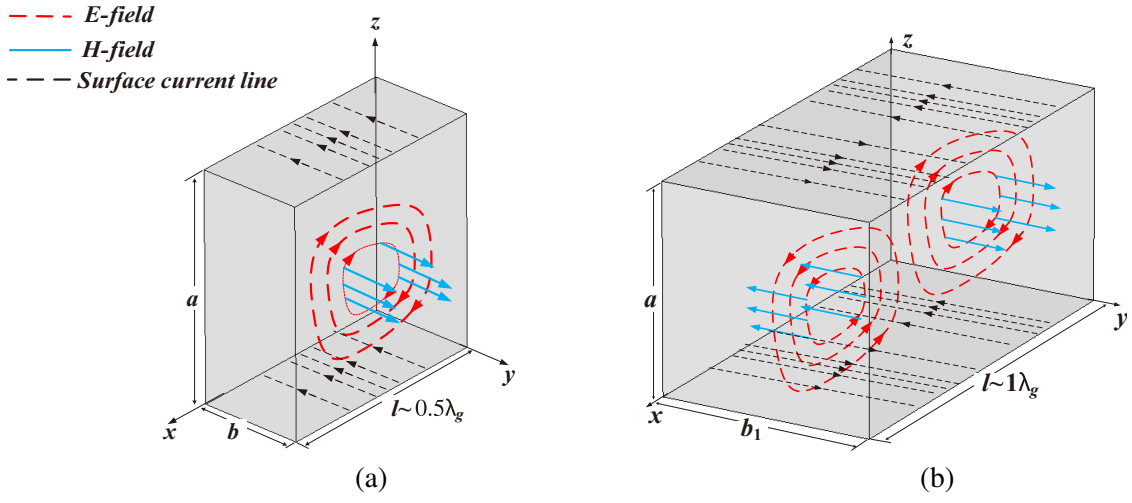

Figure 2. (a) The TE_{101} mode cavity resonator. (b) The TE_{102} mode cavity resonator.

2.3. Parametric Extraction and Performance

To obtain the desired performance of the 2×2-element subarray shown in Fig. 1(b), the matrix elements (m_{12}, $q_{e1} = q_{rn}$) values found in Equation (3) can be used to extract the subarray physical dimensions

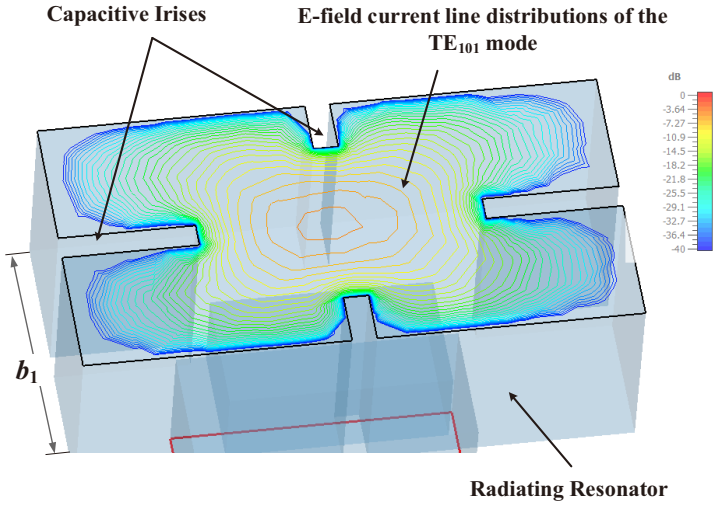

Figure 3. The current line distribution of the E-field at the center frequency 10 GHz obtained from CST simulator.

using the technique given in [14] with the aid of CST and HFSS studios. The non-scaled external quality factor (Q_{e1}) is related to the q_{e1} factor by ($q_{e1} = Q_{e1}$ FBW) where (Q_{e1}) can be computed using the following relations:

$$Q_{e1} = \frac{f_0}{\Delta f_{3\,\mathrm{dB}}} \tag{5}$$

where (f_0) is the resonant frequency, and $\Delta f_{3\,\mathrm{dB}}$ is the bandwidth obtained from the transmission (S_{21}) response of resonator 1 when it is weakly coupled to the output port. The resonator length (l_1) is utilized to control and keep f_0 at 10 GHz, while the iris width (d_0) is to control $\Delta f_{3\,\mathrm{dB}}$ and obtain the desired ($Q_{e1} = 7.610$) value.

The non-scaled coupling coefficient (M_{12}) is related to the (m_{12}) by ($m_{12} = M_{12}/\mathrm{FBW}$), where ($M_{12}$) can be computed using the following relations:

$$M_{12} = \frac{f_2^2 - f_1^2}{f_2^2 + f_1^2} \tag{6}$$

where (f_1, f_2) are resonant frequencies of resonator 1 and radiating resonator, and they are coupled to each other via the inductive iris denoted by (l_a). The resonator lengths (l_1, l_2) are manipulated to tune the frequency response to the desirable frequency band of interest (9–11 GHz), whereas the coupling iris length (l_a) is to control the passband bandwidth and obtain the desirable ($M_{12} = 0.2597$) value.

The non-scaled radiation quality factor (Q_{rn}) is related to (q_{rn}) by ($q_{rn} = Q_{rn}$ FBW), where (Q_{rn}) can be computed using the following relations [25]:

$$Q_{rn} = \frac{1}{|\Delta f_a|}\left[\frac{|S_{11}(f_a)|^2\,(1+\beta)^2 - (1-\beta)^2}{1 - |S_{11}(f_a)|^2}\right]^{1/2} \tag{7}$$

where ($\Delta f_a = 1 - (f_0^2/f_a^2)$. f_a is a frequency point around the passband edges. β is the coupling coefficient between the radiating resonator aperture and space. The radiating resonator length (l_2) is used to keep and control Δf_a of the aperture within the operating frequency range, while the radiating aperture dimensions (S_l, S_w) are to obtain the desirable ($Q_r = 7.610$) value.

The initial (d_0, l_a, l_1, l_2, S_w, and S_l) values, which are extracted using the technique presented in [14] and discussed above, are optimized in order to meet the desired simulated frequency response using both the CST and HFSS simulators [26, 27]. They are summarised and listed in Table 1.

The proposed 2 × 2 subarray antenna is simulated with radiation pattern in CST as shown in Fig. 4. The simulated S_{11} responses are compared with the calculation in Fig. 5, and they are in very

Table 1. Physical dimensions of the **2 × 2** subarray.

Parameters	Dimensions	Values (mm)
$a \times b$	Waveguide dimensions	22.86 × 10.16
d_0	Input capacitive iris width	5.64
l_1	First resonator length	20.13
l_a	Coupling inductive iris length	18.8
t_r	Coupling iris thickness	8.0
l_2	Radiating resonator length	46.0
b_1	Radiating resonator width	24.0
l_i, l_w	Irises dimensions	11.7, 4.0
t	Iris thickness	2.0
S_l, S_w	Radiating aperture dimensions	20.7, 11.0
x, y	Radiating aperture spacing	25.3, 13.0

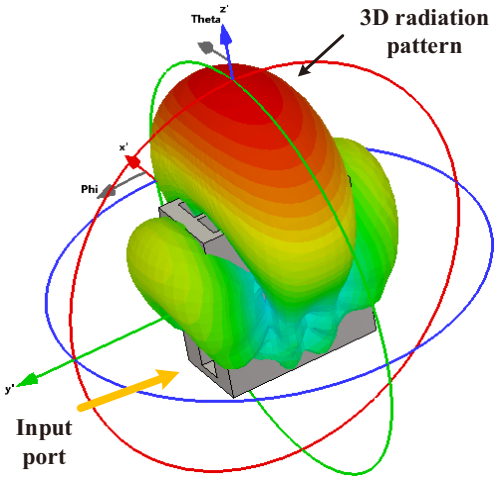

Figure 4. The proposed 2 × 2 subarray antenna modelled in CST with simulated 3D radiation pattern at 10 GHz.

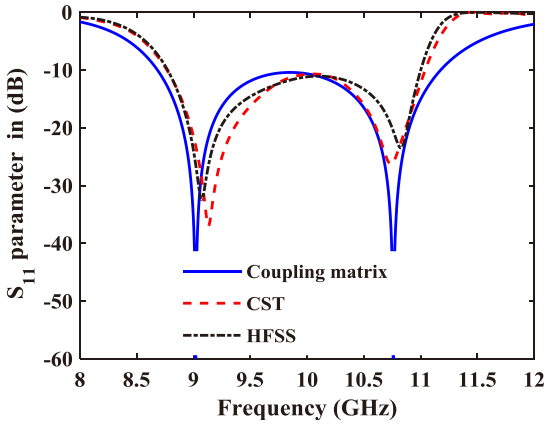

Figure 5. Calculated and simulated S_{11} response of the 2 × 2 subarray topology.

good agreement with the calculation. The simulated antenna realised gain is shown in Fig. 6. A very stable gain is obtained over the frequency range 8.9–11.1 GHz with a peak gain value of 13.1 dBi at 11 GHz. The 3-dB gain-bandwidth at center frequency 10 GHz is more than 26%, while the impedance bandwidth is around 23% at $S_{11} = -10$ dB. The dimensions of the coupling aperture (l_a, a) and radiating apertures (S_w, S_l) limit the bandwidth further. The realised gain start band attenuation is poorer than the stopband. This is due to the nature of capacitive iris employed in the structure which brings the cut-off frequency of the TE_{101} mode close to edge of the start band [15, 21]. In addition to that, the transmission zero appearing around 11.5 GHz is due to the direct coupling which could exist between the resonator 1 and the radiation ports. Such direct coupling generates phase difference and then create such kind of transmission zeros [28]. The total efficiency including the conductor loss is more than 95% over the bandwidth of interest as can be depicted in Fig. 7. The predicted radiation patterns for the E- and H-planes at frequencies 9.0, 10.0, 11.0 GHz are shown in Fig. 8. They are almost stable and independent of the frequency variations over the bandwidth of interest. The E-plane side lobe level is suppressed below −23 dB due to smaller non-radiation area and small spacing ($0.43\lambda_0$) between the radiating apertures in the E-plane. Additionally, the small non-radiating area in the E-plane leads to

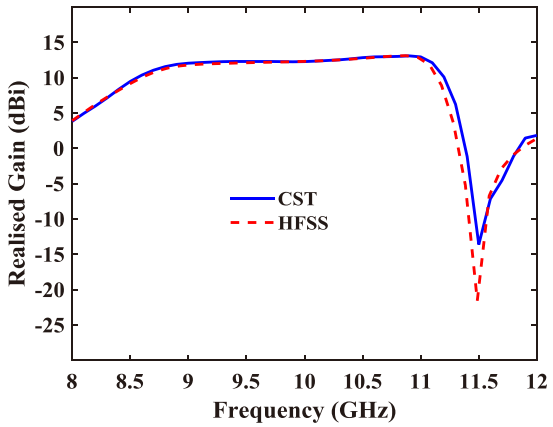

Figure 6. Simulated realised gain response of the 2×2 subarray topology.

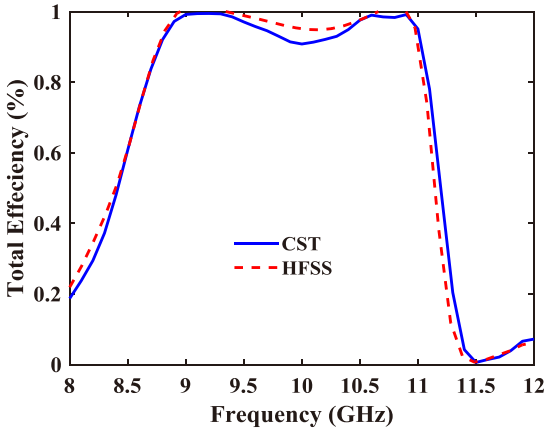

Figure 7. Simulated total efficiency response of the 2×2 subarray topology.

Table 2. Comparison with some other 2×2 subarrays.

Refs.	Types	Number of elements	Frequency (f_0) (GHz)	Volume (λ_0^3)	Bandwidth (%) $S_{11} = -10$ dB	peak gain (dBi)
[29]	Hollow-waveguide (Truncated aperture based)	2×2	32	$1.93 \times 1.92 \times 1.97 = 7.30$	1.40	14.4
[1]	Hollow-waveguide (Hexagonal aperture based)	2×2	61.5	$1.49 \times 1.89 \times 1.86 = 5.23$	14.5	NA
[30]	Microstrip array (Rectangular patch based)	2×2	5.3	NA	17.7	13.5
[10]	Hollow-waveguide (Cavity-backed aperture based)	2×2	15	NA	11.3	15.3
[12]	Hollow-waveguide (Cavity-backed rectangular aperture based)	2×2	10.25	$1.36 \times 2.92 \times 2.92 = 11.62$	14	~ 14
[31]	Microstrip array (Rectangular patch based)	2×2	5	NA	3	9.6
[16]	Rectangular waveguide cavity (rectangular aperture based (topology-I))	2×2	10	$2.31 \times 1.94 \times 1.36 = 6.09$	13.5	14.23
[16]	Rectangular waveguide cavity (rectangular aperture based (topology-II))	2×2	10	$2.40 \times 1.17 \times 1.19 = 3.34$	13.2	12.94
This work	**Rectangular waveguide cavity rectangular aperture based**	**2×2**	**10**	**$2.0 \times 1.66 \times 0.933 = 3.09$**	**23**	**13.1**

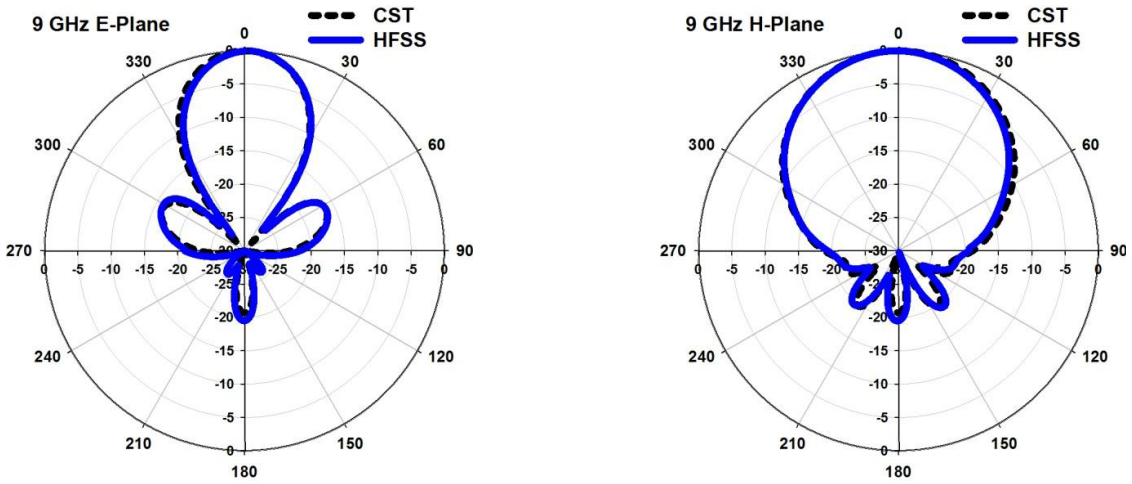

(a)

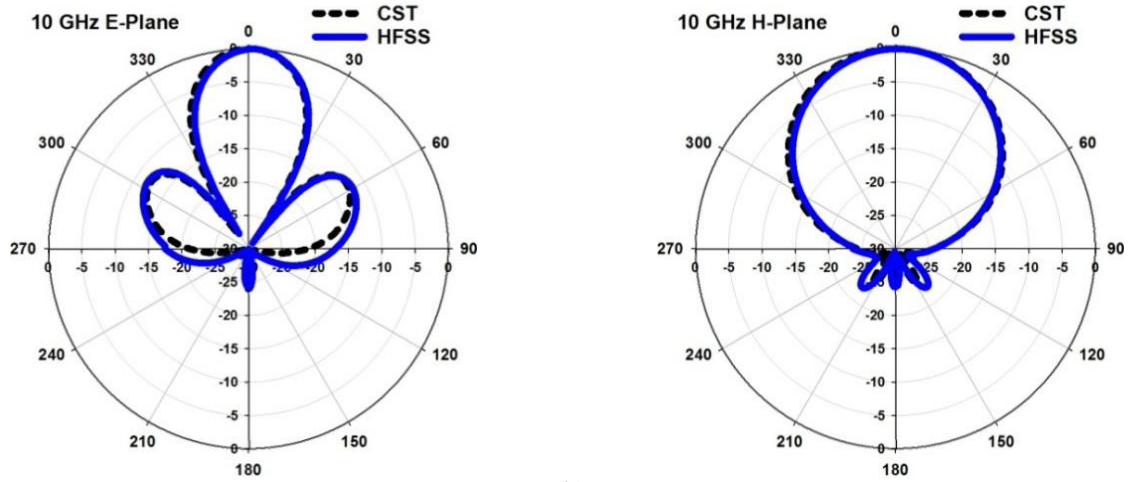

(b)

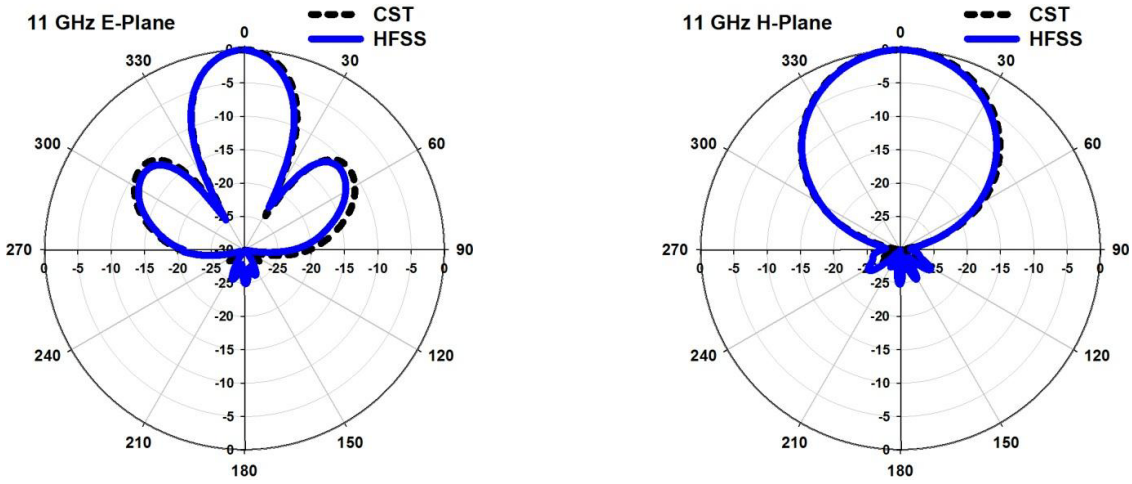

(c)

Figure 8. Simulated E- and H-planes radiation pattern responses of the 2×2 subarray topology at 9.0, 10.0, and 11.0 GHz.

reducing the radiation pattern beamwidth and making the pattern more directive as well.

To evaluate the performance and structural characteristics of the proposed 2×2 subarray antenna, a comparison between the proposed 2×2 subarray and previous 2×2 subarrays is made in Table 2. A 2×2 filtering subarray, which truncated the apertures to achieve high gain and circularly polarized presented in [29], was realised by employing five resonators. However, our design has employed only two resonators and has wider bandwidth and smaller volume. A principal 2×2 unit array, which consists of four hexagonal apertures formed from plate-laminated waveguide, is presented in [1]. It is not competitive to the proposed 2×2 subarray, particularly in terms of volume and bandwidth. Finally, it is important to mention that the proposed subarray exhibits wider bandwidth, small volume, and lower sidelobe levels than the results presented in [10, 12, 16, 30–32].

3. CONCLUSIONS

A novel topology for the design of a 2×2-element subarray antenna has been proposed. Rectangular waveguide resonators were employed to incorporate the topology and configure the physical structure. The configured structure has the flexibility in reducing the subarray size and the inter-element spacing which leads to suppressing the side lobe levels significantly. The coupling matrix approach was utilized to calculate the reflection coefficient. the simulations results obtained by CST and Anosft HFSS were in very good agreement with the calculation. The subarray has a very stable gain with less than 0.5 dBi fluctuation over the bandwidth of interest (9–11 GHz), with a peak gain value of 13.1 dBi at 11 GHz. A very large impedance bandwidth, which is more than 23% at $f_0 = 10$ GHz when $S_{11} = -10$ dB, was obtained.

ACKNOWLEDGMENT

The authors would like to thank the Emerging Device Technology (EDT) research group at the University of Birmingham, UK for all support regarding the simulation softwares.

Funding: This research did not receive any specific grant from funding agencies in the public, commercial, or not-for-profit sectors.

Institutional review board statement: Not applicable.

Informed consent statement: Not applicable.

Data availability statement: All codes and algorithms will be made available on request to the correspondent author's email with appropriate justification.

Declaration of competing interest: The authors declare that they have no known competing financial interests or personal relationships that could have appeared to influence the work reported in this paper.

REFERENCES

1. Zhang, M., T. Yamamoto, J. Hirokawa, and M. Ando, "A wideband circularly polarized corporate-fed waveguide aperture array in the 60 GHz band," *IEEE Antennas and Wireless Propagation Letters*, Vol. 20, 1824–1828, 2021.
2. Volakis, J. L., *Antenna Engineering Handbook*, McGraw-Hill Education, 2007.
3. Miura, Y., J. Hirokawa, M. Ando, Y. Shibuya, and G. Yoshida, "Double-layer full-corporate-feed hollow-waveguide slot array antenna in the 60-GHz band," *IEEE Transactions on Antennas and Propagation*, Vol. 59, 2844–2851, 2011.
4. Ando, M., Y. Tsunemitsu, M. Zhang, J. Hirokawa, and S. Fujii, "Reduction of long line effects in single-layer slotted waveguide arrays with an embedded partially corporate feed," *IEEE Transactions on Antennas and Propagation*, Vol. 58, 2275–2280, 2010.

5. Arakawa, H., H. Irie, T. Tomura, and J. Hirokawa, "Suppression of E-plane sidelobes using a double slit layer in a corporate-feed waveguide slot array antenna consisting of 2×2-element radiating units," *IEEE Transactions on Antennas and Propagation*, Vol. 67, 3743–3751, 2019.
6. Tekkouk, K., J. Hirokawa, K. Oogimoto, T. Nagatsuma, H. Seto, Y. Inoue, et al., "Corporate-feed slotted waveguide array antenna in the 350-GHz band by silicon process," *IEEE Transactions on Antennas and Propagation*, Vol. 65, 217–225, 2016.
7. Shad, S. and H. Mehrpouyan, "60 GHz waveguide-fed cavity array antenna by multistepped slot aperture," *IEEE Antennas and Wireless Propagation Letters*, Vol. 19, 438–442, 2020.
8. Kim, D., J. Hirokawa, M. Ando, J. Takeuchi, and A. Hirata, "4×4-element corporate-feed waveguide slot array antenna with cavities for the 120 GHz-band," *IEEE Transactions on Antennas and Propagation*, Vol. 61, 5968–5975, 2013.
9. Tomura, T., Y. Miura, M. Zhang, J. Hirokawa, and M. Ando, "A 45° linearly polarized hollow-waveguide corporate-feed slot array antenna in the 60-GHz band," *IEEE Transactions on Antennas and Propagation*, Vol. 60, 3640–3646, 2012.
10. Huang, G.-L., S.-G. Zhou, T.-H. Chio, and T.-S. Yeo, "Broadband and high gain waveguide-fed slot antenna array in the Ku-band," *IET Microwaves, Antennas & Propagation*, Vol. 8, 1041–1046, 2014.
11. Hirokawa, J., "Plate-laminated waveguide slot array antennas and its polarization conversion layers," *Automatika: časopis za automatiku, mjerenje, elektroniku, računarstvo i komunikacije*, Vol. 53, 9–19, 2012.
12. Chen, Z., S.-G. Zhou, and T.-H. Chio, "A class of all metal cavity-backed slot array with direct metal laser sintering," *IEEE Access*, Vol. 6, 69650–69659, 2018.
13. He, J., Y. Wu, D. Chen, M. Zhang, J. Hirokawa, and Q. Liu, "Realization of a wideband series-fed 4×4-element waveguide slot array in the X-band," *IEEE Access*, 2021.
14. Mahmud, R. H. and M. J. Lancaster, "High-gain and wide-bandwidth filtering planar antenna array-based solely on resonators," *IEEE Transactions on Antennas and Propagation*, Vol. 65, 2367–2375, 2017.
15. Mahmud, R. H., H. N. Awl, Y. I. Abdulkarim, M. Karaaslan, and M. J. Lancaster, "Filtering two-element waveguide antenna array based on solely resonators," *AEU-International Journal of Electronics and Communications*, Vol. 121, 153232, 2020.
16. Mahmud, R. H. and M. J. Lancaster, "A 2×2 filtering subarray element antennas using all-resonator structures," *IET Microwaves, Antennas & Propagation*, Vol. 15, 592–599, 2021.
17. Mahmud, R. H., "Synthesis of waveguide antenna arrays using the coupling matrix approach," University of Birmingham, 2016.
18. Williams, A. E., "A four-cavity elliptic waveguide filter," *IEEE Transactions on Microwave Theory and Techniques*, Vol. 18, 1109–1114, 1970.
19. Atia, A. E. and A. E. Williams, "Narrow-bandpass waveguide filters," *IEEE Transactions on Microwave Theory and Techniques*, Vol. 20, 258–265, 1972.
20. Skaik, T. F., M. Lancaster, and F. Huang, "Synthesis of multiple output coupled resonator circuits using coupling matrix optimisation," *IET Microwaves, Antennas & Propagation*, Vol. 5, 1081–1088, 2011.
21. Shang, X., Y. Wang, W. Xia, and M. J. Lancaster, "Novel multiplexer topologies based on all-resonator structures," *IEEE Transactions on Microwave Theory and Techniques*, Vol. 61, 3838–3845, 2013.
22. Hong, J.-S. G. and M. J. Lancaster, *Microstrip Filters for RF/Microwave Applications*, Vol. 167, John Wiley & Sons, 2004.
23. Pozar, D. M., *Microwave Engineering*, Chap. 6, John Wiley & Sons, 2011.
24. Miek, D., C. Bartlett, F. Kamrath, P. Boe, and M. Höft, "Investigation of the cutting plane and tolerance analysis of cross-coupled W-band waveguide filters with multiple transmission zeros by source to load cross-coupling," *International Journal of Microwave and Wireless Technologies*, 1–10, 2021.

25. Lancester, M., *Passive Microwave Device Applications of Superconductors*, Cambridge University Press, Cambridge, UK, 1997.
26. C. M. Studio, Computer Simulation Technology AG, Darmstadt, Germany, 2009.
27. El Mrabet, O., "High frequency structure simulator (HFSS) tutorial," *IETR, UMR CNRS*, Vol. 6164, 2005–2006, 2006.
28. Carceller, C., P. Soto, V. Boria, M. Guglielmi, and J. Gil, "Design of compact wideband manifold-coupled multiplexers," *IEEE Transactions on Microwave Theory and Techniques*, Vol. 63, 3398–3407, 2015.
29. Zhang, Y., J. Xu, X. He, F. Zhang, Y. Sun, X. Li, et al., "A 3-D printed circularly polarized filtering antenna," *2019 IEEE International Symposium on Antennas and Propagation and USNC-URSI Radio Science Meeting*, 1999–2000, 2019.
30. Santosa, C. E., J. T. S. Sumantyo, C. M. Yam, K. Urata, K. Ito, and S. Gao, "Subarray design for C-band circularly-polarized synthetic aperture radar antenna onboard airborne," *Progress In Electromagnetics Research*, Vol. 163, 107–117, 2018.
31. Lin, C.-K. and S.-J. Chung, "A filtering microstrip antenna array," *IEEE Transactions on Microwave Theory and Techniques*, Vol. 59, 2856–2863, 2011.
32. Mansour, G., M. J. Lancaster, P. S. Hall, P. Gardner, and E. Nugoolcharoenlap, "Design of filtering microstrip antenna using filter synthesis approach," *Progress In Electromagnetics Research*, Vol. 145, 59–67, 2014.